Hindawi
Shock and Vibration
Volume 2018, Article ID 4957917, 11 pages
https://doi.org/10.1155/2018/4957917

Research Article

Zonal Disintegration Mechanism of Deep Rock Masses under Coupled High Axial Geostress and Blasting Load

Pu Yuan [1,2] **and Ying Xu** [1,2,3]

[1] *School of Civil Engineering and Architecture, Anhui University of Science and Technology, Huainan 232001, China*
[2] *Engineering Research Center of Underground Mine Construction, Ministry of Education, Anhui University of Science and Technology, Huainan 232001, China*
[3] *State Key Laboratory of Deep Coal Mining and Environment Protection, Huainan Mining Group Co., Ltd., Huainan 232001, China*

Correspondence should be addressed to Pu Yuan; puy2012@126.com

Received 7 March 2018; Revised 27 May 2018; Accepted 4 June 2018; Published 4 July 2018

Academic Editor: Yuri S. Karinski

Zonal disintegration phenomenon with alternative distribution of fracture zones and nonfracture zones is a characteristic failure in deep rock masses, especially for deep tunnel excavated by drill and blast method. To investigate the mechanism of zonal disintegration under coupled high axial geostress and blasting load, elastic stress field distribution for a circular tunnel in deep isotropic rock masses is obtained. Furthermore, Hoek-Brown criterion is amended by considering blast-induced damage effect. Both radial blasting load and blast-induced damage effect are assumed to decay in a negative exponential function. Taking the deep tunnel of Dingji coal mine in China as engineering background, the number and width of fracture zones are determined by deduced elastic stress field and modified Hoek-Brown criterion. Then numerical computation is conducted. Numerical computation results indicate that both the number and width of fracture zones mainly depend on high axial geostress and mechanical parameters of deep rock masses, and peak radial blasting load plays an important role in determining the width of fracture zone near the excavation.

1. Introduction

With the ever-increasing demand of energy resources, deep mineral resources exploitation is inevitable and imperative due to the continuing consumption of shallow mineral resources [1], and deep mining has been identified as an important topic for research under China's State Key Research and Development Program [2]. During deep mineral resources exploitation, some special rock failure phenomena, such as zonal disintegration and rockburst, are frequently reported and quite different from those in shallow rock Engineering [3–5]. Among these special rock failure phenomena, zonal disintegration is such a unique phenomenon with alternative distribution of fracture zones and nonfracture zones around an excavation in deep rock mass [6, 7].

Zonal disintegration phenomenon is considered as one of the characteristics of deep rock masses. In 1970s, zonal disintegration phenomenon was firstly observed ahead of stope faces by periscope in Doornfontein gold mine of South Africa at about -2300 m level [8]. Then zonal disintegration phenomenon was also monitored around underground workings by electrometric techniques in Oktyabrsky Mine and Taymyrsky Mine of Russia at about -1000 m level [9]. However, an obvious zonal disintegration phenomenon in China was detected by bore TV video in Huainan mine at -910 m level [10].

Formation condition and mechanism of zonal disintegration under in situ stresses have been studied subsequently by theoretical analysis, model experiment, numerical simulation, and in situ monitoring. Shemyakin et al. [11] considered that the fracture zone is the splitting failure in rock mass. Odintsev [12] found that zonal disintegration can be predicted by spatial periodicity of splitting failure around an excavation. Zhang et al. [13] established an elastic damage-softening model for zonal disintegration according to strain gradient theory and continuum damage mechanics. Chen et al. [5] revealed that the circulation of fracture zone is mainly caused by the peak stress intensity factor of a "new" plastic boundary. Jia et al. [14] stated that failure patterns of

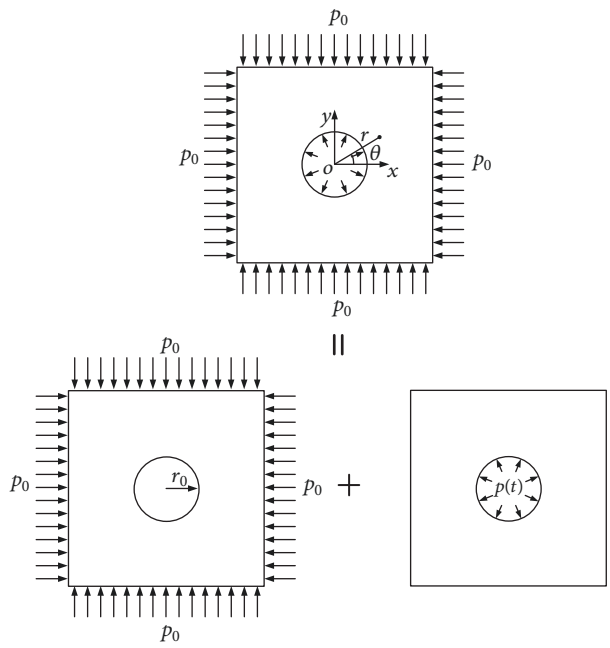

Figure 1: Decomposition of elastic stress field under coupled high axial geostress and blasting load.

surrounding rock mass are influenced by multiaxial stress state and a high axial geostress is essential for zonal disintegration. Yuan and Gu [15] indicated that the major radial tension strain following tension breakage is the key factor of zonal disintegration. While traditional static mechanics theory cannot illustrate the formation of zonal disintegration well, therefore the unloading effect during excavation process is considered. Zhu et al. [16] indicated that a slowly unloading P-wave reflecting from a free surface may induce zonal disintegration. By assuming deep rock masses containing a set of parallel cracks, zonal disintegration mechanism was analyzed and fracture zone occurred when cracks satisfy the crack grown criterion or the strain energy density factor theory [17, 18].

Based on non-Euclidean model, zonal disintegration mechanism around a deep circular tunnel was investigated and elastic stress field of surrounding rock was derived under various conditions, such as nonhydrostatic pressure state and dynamic unloading. In non-Euclidean model, radial stress and tangential stress around deep tunnel were obviously fluctuant, which was quite different with classic elastic solution [19, 20]. And zonal disintegration around an excavation is the result of the alternate appearance of stress wave crests and troughs [21, 22]. By establishing a new non-Euclidean model in a nonhydrostatic pressure state, it was found that the magnitude and position of fracture zones depend on the actual geostress state and non-Euclidean parameters [23]. Considering the characteristics of rock mass, both crack-weakened rock mass and cross-anisotropic rock mass were analyzed for zonal disintegration with a non-Euclidean model [24, 25]. Moreover, zonal disintegration around a deep circular tunnel under dynamic unloading condition was also studied with non-Euclidean model [26, 27]. When considering the excavation unloading effect, it was found that the magnitude and position of fracture zone mainly depend on unloading rate, and the quantity of fracture zones increases with decreasing excavation time [18, 22].

In consideration of complex geological environment and blasting excavation, rock failure in deep rock mass can be induced by blasting load [28, 29]. General Particle Dynamics (GPD) method was put forward to study the zonal disintegration mechanism of deep rock mass in blasting excavation, and it was found that dynamic loads and high geostress are two dominant factors for occurrence of zonal disintegration [30]. Blasting excavation not only applies a dynamic load on deep rock masses but also induces blasting damage around an excavation [31, 32]. By considering both high axial geostress and blasting load in deep rock masses, failure mechanism of zonal disintegration is investigated by elastic stress field analyses and modified Hoek-Brown criterion. Then the effects of high axial geostress, mechanical parameters of deep rock masses, and radial blasting load on zonal disintegration are analyzed.

2. Elastic Stress Field under Coupled High Axial Geostress and Blasting Load

2.1. Decomposition of Elastic Stress Field. It is found that the axial stress of tunnel is vital for zonal disintegration [33]. Therefore, high axial geostress should be considered during elastic stress field analyses.

It is assumed that a deep circular tunnel, whose radius is r_0, is subjected to a vertical geostress p_0, a horizontal geostress p_0 at infinity, and a high axial geostress p_z along the tunnel axis. Under coupled high axial geostress and blasting load, elastic stress field around a circular excavation in deep rock mass can be divided into two parts, elastic stress field caused by high axial geostress and transient elastic stress field induced by blasting load, which can be seen from Figure 1.

2.2. Elastic Stress Field Caused by High Axial Geostress. To simplify the analyses, three-dimensional problem is converted into a quasi-plane strain problem with an initial axial strain ε_{z0} [34]. According to simplified quasi-plane strain state, axial stress component σ_z can be expressed as

$$\sigma_z = E\varepsilon_{z0} + \mu\left(\sigma_r + \sigma_\theta\right) \tag{1}$$

where E is Young's modulus, μ is Poisson's ratio, and σ_r and σ_θ are radial stress component and tangential stress component, respectively.

As $r \longrightarrow \infty$, $\sigma_z \longrightarrow p_z$, $\sigma_r \longrightarrow p_0$, and $\sigma_\theta \longrightarrow p_0$, the initial axial strain ε_{z0} can be obtained as

$$\varepsilon_{z0} = \frac{\left(p_z - 2\mu p_0\right)}{E} \tag{2}$$

According to the research of Qian et al. [34], the first invariant of stress tensor I_1 in surrounding rock with a distance r from tunnel center can be obtained as

$$\begin{aligned} I_1 = &-\frac{E}{2\rho\left(1-\mu\right)}\left[AJ_0\left(\rho^{1/2}r\right) + BN_0\left(\rho^{1/2}r\right)\right. \\ &\left. - CK_0\left(\rho^{1/2}r\right)\right] + p_z + 2p_0 \end{aligned} \tag{3}$$

$$\begin{aligned} A = &\left(\frac{C}{2}\right)\pi\rho^{1/2}r_0\left[K_0\left(\rho^{1/2}r_0\right)N_1\left(\rho^{1/2}r_0\right)\right. \\ &\left. - K_1\left(\rho^{1/2}r_0\right)N_0\left(\rho^{1/2}r_0\right)\right] \end{aligned} \tag{4}$$

$$\begin{aligned} B = &\left(\frac{C}{2}\right)\pi\rho^{1/2}r_0\left[K_0\left(\rho^{1/2}r_0\right)J_1\left(\rho^{1/2}r_0\right)\right. \\ &\left. - K_1\left(\rho^{1/2}r_0\right)J_0\left(\rho^{1/2}r_0\right)\right] \end{aligned} \tag{5}$$

$$\rho^2 = \frac{E\mu}{2q\left(1-\mu^2\right)} \tag{6}$$

where q in non-Euclidean model is the fitting parameter determined by experimental data, $J_0(\rho^{1/2}r)$ and $J_1(\rho^{1/2}r)$ are zero-order and first-order Bessel function, $N_0(\rho^{1/2}r)$ and $N_1(\rho^{1/2}r)$ are zero-order and first-order Neumann function, $K_0(\rho^{1/2}r)$ and $K_1(\rho^{1/2}r)$ are zero-order and first-order modified Bessel function of second kind, and C coincides with the Wronskian of linearly independent solutions $J_0(\rho^{1/2}r)$ and $N_0(\rho^{1/2}r)$.

According to elasticity mechanics, the first invariant of stress tensor I_1 in surrounding rock with a distance r from tunnel center can also be written as

$$\begin{aligned} I_1 &= \sigma_{z1} + \sigma_{r1} + \sigma_{\theta1} = E\varepsilon_{z0} + \mu\left(\sigma_{r1} + \sigma_{\theta1}\right) + \sigma_{r1} + \sigma_{\theta1} \\ &= E\varepsilon_{z0} + \left(1+\mu\right)\left(\sigma_{r1} + \sigma_{\theta1}\right) \end{aligned} \tag{7}$$

Then, the tangential stress component $\sigma_{\theta1}$ can be given as follows:

$$\sigma_{\theta1} = \frac{I_1 - E\varepsilon_{z0}}{1+\mu} - \sigma_{r1} \tag{8}$$

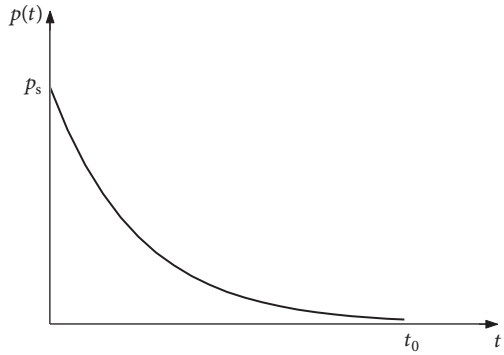

Figure 2: Time-varying radial blasting load.

Under high axial geostress, the equation of equilibrium can be expressed as

$$\frac{\partial\sigma_r}{\partial r} + \frac{2\sigma_r}{r} - \frac{I_1 - E\varepsilon_{z0}}{\left(1+\mu\right)r} = 0 \tag{9}$$

Integrating (9), the radial stress component σ_{r1} can be expressed as

$$\begin{aligned} \sigma_{r1} = &\left(1 - \frac{{r_0}^2}{r^2}\right)p_0 - \frac{E}{2\rho^{3/2}\left(1-\mu^2\right)r}\left[AJ_1\left(\rho^{1/2}r\right)\right. \\ &\left. + BN_1\left(\rho^{1/2}r\right) - CK_1\left(\rho^{1/2}r\right)\right] \end{aligned} \tag{10}$$

Substituting (10) into (8), the tangential stress component $\sigma_{\theta1}$ can be expressed as

$$\begin{aligned} \sigma_{\theta1} = &\left(1 + \frac{{r_0}^2}{r^2}\right)p_0 - \frac{E}{2\rho\left(1-\mu^2\right)}\left[AJ_0\left(\rho^{1/2}r\right)\right. \\ &\left. + BN_0\left(\rho^{1/2}r\right) - CK_0\left(\rho^{1/2}r\right)\right] \\ &+ \frac{E}{2\rho^{3/2}\left(1-\mu^2\right)r}\left[AJ_1\left(\rho^{1/2}r\right) + BN_1\left(\rho^{1/2}r\right)\right. \\ &\left. - CK_1\left(\rho^{1/2}r\right)\right] \end{aligned} \tag{11}$$

2.3. Transient Elastic Stress Field Induced by Radial Blasting Load. Elastic stress field induced by blasting load can be treated as an axial symmetric problem in plain strain state for long circular tunnel. As an impact load, blasting load usually increases firstly and then decreases. But the main cause of zonal disintegration phenomenon in deep rock mass is the tensile failure of surrounding rock in radial direction [15]. And the tensile failure in radial direction usually occurs in unloading stage rather than in loading stage. Therefore, a monotone decreasing radial blasting load $p(t)$ is applied on the boundary of circular tunnel in consideration of blasting load in excavation [35]. As shown in Figure 2, radial blasting load decays in a negative exponential function with action

time. And the expression for time-varying radial blasting load $p(t)$ is shown as follows.

$$p(t) = p_s e^{-at} \quad 0 < t \le t_0 \tag{12}$$

$$p_s = \frac{\rho_0 D^2}{160} \tag{13}$$

where p_s is the peak pressure of radial blasting load, a is exponential decay coefficient, and t_0 is the action time of radial blasting load. ρ_0 and D are density and detonation velocity of explosive.

Under blasting load, the equations of equilibrium can be written as

$$\frac{\partial^2 u(r,t)}{\partial^2 r} + \frac{1}{r}\frac{\partial u(r,t)}{\partial r} - \frac{u(r,t)}{r^2} = \frac{1}{C_p^2}\frac{\partial^2 u(r,t)}{\partial^2 t} \tag{14}$$

where C_p is longitudinal wave velocity: $C_p = \sqrt{E(1-\mu)/[\rho_0(1+\mu)(1-2\mu)]}$.

With the help of *Laplace* transform, the *Laplace* transform of $u(r,t)$ can be expressed as

$$U(r,p) = L[u(r,t)] = \int_0^\infty u(r,t)\, e^{-pt} dt \tag{15}$$

where p is parameter of *Laplace* transform.

Then the equations of equilibrium can be written as

$$\frac{\partial^2 U(r,p)}{\partial^2 r} + \frac{1}{r}\frac{\partial U(r,p)}{\partial r} - \frac{U(r,p)}{r^2} = \frac{p^2}{C_p^2} U(r,p) \tag{16}$$

Assuming that $\eta = pr/C_p$, (16) can be obtained as

$$\eta^2 \frac{\partial^2 U(\eta,p)}{\partial^2 \eta} + \eta \frac{\partial U(\eta,p)}{\partial \eta} - \left(\eta^2 + 1\right) U(\eta,p) = 0 \tag{17}$$

Equation (17) is modified Bessel equation, and its general solution is

$$U(\eta,p) = MI_1(\eta) + NK_1(\eta) \tag{18}$$

$$I_1(\eta) = \sum_{k=0}^{\infty} \frac{1}{k!\Gamma(k+2)} \left(\frac{\eta}{2}\right)^{2k+1} \tag{19}$$

$$K_1(\eta) = \lim_{\alpha \longrightarrow 1} \frac{I_{-\alpha}(\eta) - I_\alpha(\eta)}{\sin \alpha\pi} \frac{\pi}{2} \tag{20}$$

where $I_1(\eta)$ and $K_1(\eta)$ are first-order modified Bessel function of first kind and second kind and M and N are the parameters determined by boundary conditions.

As $\alpha \longrightarrow 1$, $K_1(\eta) \longrightarrow \infty$. While $U(\eta, p)$ is bounded, the parameter N is equal to 0. According to the asymptotic property of Bessel function, the first-order modified Bessel function of first kind $I_1(\eta)$ can be expressed as

$$I_1(\eta) = \frac{1}{\sqrt{2\pi\eta}} e^{\eta} \tag{21}$$

Therefore, (18) can be written as

$$U(\eta,p) = \frac{M}{\sqrt{2\pi\eta}} e^{\eta} \tag{22}$$

According to generalized Hooke's law, the strain for plain strain problem in axisymmetric condition can be calculated as

$$\varepsilon_r = \frac{1-\mu^2}{E}\left(\sigma_{r2} - \frac{\mu}{1-\mu}\sigma_{\theta 2}\right) \tag{23}$$

$$\varepsilon_\theta = \frac{1-\mu^2}{E}\left(\sigma_{\theta 2} - \frac{\mu}{1-\mu}\sigma_{r2}\right) \tag{24}$$

By adding (23) multiplied by (1-μ)/μ with (24), the following can be obtained:

$$\begin{aligned} \varepsilon_r \frac{1-\mu}{\mu} + \varepsilon_\theta &= \frac{1-\mu^2}{E}\frac{1-\mu}{\mu}\left(\sigma_{r2} - \frac{\mu}{1-\mu}\sigma_{\theta 2}\right) \\ &\quad + \frac{1-\mu^2}{E}\left(\sigma_{\theta 2} - \frac{\mu}{1-\mu}\sigma_{r2}\right) \\ &= \frac{(1+\mu)(1-2\mu)}{E\mu}\sigma_{r2} \end{aligned} \tag{25}$$

Then, the radial stress component σ_{r2} can be rewritten as

$$\sigma_{r2} = \frac{E(1-\mu)}{(1+\mu)(1-2\mu)}\varepsilon_r + \frac{E\mu}{(1+\mu)(1-2\mu)}\varepsilon_\theta \tag{26}$$

By adding (23) multiplied by μ with (24) multiplied by (1-μ), the following can be obtained:

$$\begin{aligned} &\varepsilon_r \mu + \varepsilon_\theta (1-\mu) \\ &\quad = \frac{1-\mu^2}{E}\mu\left(\sigma_{r2} - \frac{\mu}{1-\mu}\sigma_{\theta 2}\right) \\ &\qquad + \frac{1-\mu^2}{E}(1-\mu)\left(\sigma_{\theta 2} - \frac{\mu}{1-\mu}\sigma_{r2}\right) \\ &\quad = \frac{(1+\mu)(1-2\mu)}{E}\sigma_{\theta 2} \end{aligned} \tag{27}$$

Then, the tangential stress component $\sigma_{\theta 2}$ can be rewritten as

$$\sigma_{\theta 2} = \frac{E\mu}{(1+\mu)(1-2\mu)}\varepsilon_r + \frac{E(1-\mu)}{(1+\mu)(1-2\mu)}\varepsilon_\theta \tag{28}$$

Assuming that $c_1 = E(1-\mu)/[(1+\mu)(1-2\mu)]$ and $c_2 = E\mu/[(1+\mu)(1-2\mu)]$, the stress-strain relation can be rewritten as

$$\sigma_{r2} = c_1\varepsilon_r + c_2\varepsilon_\theta = c_1\frac{\partial u(r,t)}{\partial r} + c_2\frac{u(r,t)}{r} \tag{29}$$

$$\sigma_{\theta 2} = c_2\varepsilon_r + c_1\varepsilon_\theta = c_2\frac{\partial u(r,t)}{\partial r} + c_1\frac{u(r,t)}{r} \tag{30}$$

On the boundary of circular tunnel, the stress boundary condition can be expressed as

$$\sigma_{r2}\big|_{r=r_0} = \left[c_1\frac{\partial u(r,t)}{\partial r} + c_2\frac{u(r,t)}{r}\right]\Bigg|_{r=r_0} = p(t) \tag{31}$$

With the help of *Laplace* transform, the stress boundary condition can be written as

$$\left[c_1\frac{\partial U(\eta,p)}{\partial\eta}+c_2\frac{U(\eta,p)}{\eta}\right]\Bigg|_{\eta=\eta_0}=P(p) \tag{32}$$

$$P(p)=L[p(t)]=\int_0^\infty p(\tau)\,e^{-pt}dt \tag{33}$$

where $\eta_0 = pr_0/C_p$.

Substituting (22) into (32), the parameter M can be obtained as

$$M=\frac{2P(p)\eta_0 C_p\sqrt{2\pi\eta_0}}{pe^{\eta_0}\left[c_1(2\eta_0-1)+2c_2\right]} \tag{34}$$

According to $\eta = pr/C_p$ and (34), (22) can be expressed as

$$U(r,p)=\frac{P(p)\sqrt{r_0/r}C_p/c_1}{\left[p-(1/2-c_2/c_1)\left(C_p/r_0\right)\right]}e^{((r-r_0)/C_p)p} \tag{35}$$

According to convolution theorem of *Laplace* transform,

$$L[f_1(t)*f_2(t)]=F_1(p)*F_2(p) \tag{36}$$

$$F_1(p)=P(p)\,e^{((r-r_0)/C_p)p} \tag{37}$$

$$F_2(p)=\frac{\sqrt{r_0/r}C_p/c_1}{\left[p-(1/2-c_2/c_1)\left(C_p/r_0\right)\right]} \tag{38}$$

With the help of inverse *Laplace* transform, the radial displacement $u(r,t)$ around circular tunnel is obtained as

$$u(r,t)=\frac{C_p p_s\sqrt{r_0/r}}{c_1}e^{((c_1-2c_2)/2c_1r_0)C_pt-a(t+(r-r_0)/C_p)} \tag{39}$$

Therefore, according to (29) and (30), the radial stress component σ_{r2} and tangential stress component $\sigma_{\theta 2}$ induced by radial blasting load can be obtained as

$$\begin{aligned}\sigma_{r2}&=c_1\frac{\partial u(r,t)}{\partial r}+c_2\frac{u(r,t)}{r}=\left[\frac{c_2C_p}{c_1}-\left(ar+\frac{C_p}{2}\right)\right]\\&\cdot\frac{p_s\sqrt{r_0/r}}{r}e^{((c_1-2c_2)/2c_1r_0)C_pt-a(t+(r-r_0)/C_p)}\\&=\left[\frac{\mu C_p}{1-\mu}-\left(ar+\frac{C_p}{2}\right)\right]\frac{p_s\sqrt{r_0/r}}{r}\\&\cdot e^{((1-3\mu)/2r_0(1-\mu))C_pt-a(t+(r-r_0)/C_p)}\end{aligned} \tag{40}$$

$$\begin{aligned}\sigma_{\theta 2}&=c_2\frac{\partial u(r,t)}{\partial r}+c_1\frac{u(r,t)}{r}\\&=\left[C_p-\frac{c_2}{c_1}\left(ar+\frac{C_p}{2}\right)\right]\frac{p_s\sqrt{r_0/r}}{r}\\&\cdot e^{((c_1-2c_2)/2c_1r_0)C_pt-a(t+(r-r_0)/C_p)}\\&=\left[C_p-\frac{\mu}{1-\mu}\left(ar+\frac{C_p}{2}\right)\right]\frac{p_s\sqrt{r_0/r}}{r}\\&\cdot e^{((1-3\mu)/2r_0(1-\mu))C_pt-a(t+(r-r_0)/C_p)}\end{aligned} \tag{41}$$

2.4. Elastic Stress Field under Coupled High Axial Geostress and Blasting Load. Consequently, the radial stress component σ_r and tangential stress component σ_θ under coupled high axial geostress and blasting load can be expressed as

$$\begin{aligned}\sigma_r&=\sigma_{r1}+\sigma_{r2}=\left(1-\frac{r_0^2}{r^2}\right)p_0\\&-\frac{E}{2\rho^{3/2}(1-\mu^2)r}\left[AJ_1\left(\rho^{1/2}r\right)+BN_1\left(\rho^{1/2}r\right)\right.\\&\left.-CK_1\left(\rho^{1/2}r\right)\right]+\left[\frac{\mu C_p}{1-\mu}-\left(ar+\frac{C_p}{2}\right)\right]\frac{p_s\sqrt{r_0/r}}{r}\\&\cdot e^{((1-3\mu)/2r_0(1-\mu))C_pt-a(t+(r-r_0)/C_p)}\end{aligned} \tag{42}$$

$$\begin{aligned}\sigma_\theta&=\sigma_{\theta1}+\sigma_{\theta2}=\left(1+\frac{r_0^2}{r^2}\right)p_0\\&+\frac{E}{2\rho^{3/2}(1-\mu^2)r}\left[AJ_1\left(\rho^{1/2}r\right)+BN_1\left(\rho^{1/2}r\right)\right.\\&\left.-CK_1\left(\rho^{1/2}r\right)\right]-\frac{E}{2\rho(1-\mu^2)}\left[AJ_0\left(\rho^{1/2}r\right)\right.\\&\left.+BN_0\left(\rho^{1/2}r\right)-CK_0\left(\rho^{1/2}r\right)\right]+\left[C_p\right.\\&\left.-\frac{\mu}{1-\mu}\left(ar+\frac{C_p}{2}\right)\right]\frac{p_s\sqrt{r_0/r}}{r}\\&\cdot e^{((1-3\mu)/2r_0(1-\mu))C_pt-a(t+(r-r_0)/C_p)}\end{aligned} \tag{43}$$

Substituting (2), (42), and (43) into (1), the axial stress component σ_z can be expressed as

$$\begin{aligned}\sigma_z&=E\varepsilon_{z0}+\mu(\sigma_r+\sigma_\theta)=p_z\\&-\frac{E\mu}{2\rho(1-\mu^2)}\left[AJ_0\left(\rho^{1/2}r\right)+BN_0\left(\rho^{1/2}r\right)\right.\\&\left.-CK_0\left(\rho^{1/2}r\right)\right]+\left(\frac{C_p}{2}-ar\right)\frac{\mu p_s\sqrt{r_0/r}}{r(1-\mu)}\\&\cdot e^{((1-3\mu)/2r_0(1-\mu))C_pt-a(t+(r-r_0)/C_p)}\end{aligned} \tag{44}$$

3. Hoek-Brown Criterion Considering Blast-Induced Damage Effect

Assume that when deep rock mass meets the nonlinear Hoek-Brown criterion, deep rock mass fracture occurs. And the size and location of fracture zone can be obtained according to principal stress components. The Hoek-Brown criterion can be expressed as [36, 37]

$$\sigma_1=\sigma_3+\sqrt{m_b\sigma_c\sigma_3+s\sigma_c^2} \tag{45}$$

where σ_1 and σ_3 are the maximum and minimum principal stress, σ_c is uniaxial compressive strength of intact rock, and m_b and s are strength parameters.

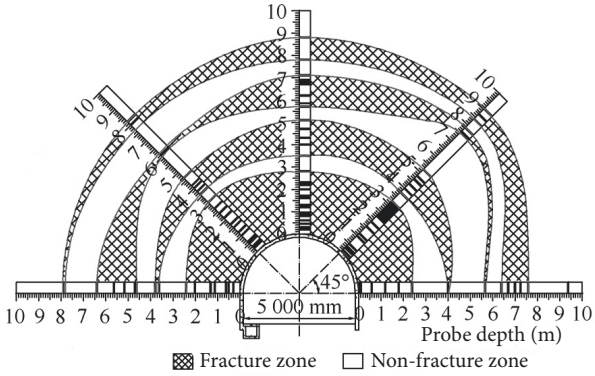

Figure 3: Zonal disintegration at Dingji mine [10].

Strength parameters m_b and s can be calculated by GSI (geological strength index). During blasting excavation, blast-induced damage plays down the integrity of rock mass and weakens the mechanical properties of rock mass. Hence, blast-induced damage factor D is introduced for cumulative damage effects of blasting excavation [38]. Then, the value of strength parameters m_b and s can be obtained as

$$m_b = m_i \exp\left(\frac{GSI - 100}{28 - 14D}\right) \quad (46)$$

$$s = \exp\left(\frac{GSI - 100}{9 - 3D}\right) \quad (47)$$

where m_i is the value of m_b for intact rock.

With the increase of distance, blast-induced damage factor D decays in a negative exponential function [38], and it can be assumed as

$$D = e^{-(r-r_0)/r_0} \quad (48)$$

4. Validation of Present Results

In China, an obvious zonal disintegration phenomenon was observed in Dingji coal mine at -910 m level. The distribution of facture zones is shown in Figure 3 [10]. According to research of Zhang et al. [39], an essential condition for zonal disintegration is maximum principal stress parallel to tunnel axis, exceeding 1.5 times uniaxial compressive strength of surrounding rock mass.

According to in situ condition, density of sandstone is 2620 kg/m^3, Young's modulus is 12.97 GPa, Poisson's ratio is 0.268, and uniaxial compressive strength is 88.55 MPa. The height and width of straight wall arch tunnel are 3.88 m and 5.00 m, respectively. According to equivalent circular method [40], the equivalent circle radius is 2.54 m. In consideration of overburden rock mass, vertical geostress and horizontal geostress p_0 at infinity are 25.10 MPa. High axial geostress p_z is assumed to be uniaxial compressive strength of surrounding rock mass, 88.55 MPa. Non-Euclidean model $q = 3.28\times10^7$ N·m^2; $C = 50$ m^{-2}. Considering rock structure, joints, and initial cracks, Hoek-Brown parameter m_i is 10, and GSI is 75. Density and detonation velocity of explosive are 1100 kg/m^3 and 3262 m/s, respectively. Peak pressure, decay coefficient, and action time of radial blasting load are 73.15 MPa, 0.87, and 8 ms, respectively. Blast-induced damage factor D decays in a negative exponential function.

Figure 4 presents the number and location of fracture zones from present numerical computation results. As seen from Figure 4, zonal disintegration arises in both conditions, while the width of fracture zones is different. On one hand, radial blasting load leads to stress redistribution around the deep tunnel. Then the elastic stress field is changed. On the other hand, radial blasting load produces some microcracks in surrounding rock with deterioration of its mechanical properties and damage to its integrity. It can be found that blasting load plays an important role in determining the width of fracture zones near the excavation. Comparing Figure 3 with Figure 4, the number and location of fractured zones under coupled high axial geostress and blasting load are in good accordance with the results observed in Dingji coal mine.

5. Numerical Computation Results

5.1. Effect of Geological Strength Index (GSI) on Distribution of Fracture Zones. Distribution of fractures zones under different geological strength index (GSI) conditions is shown in Figure 5. The other parameters are the same as mentioned in Section 4.

As seen from Figure 5, both the number and the width of fracture zones increase with the reduction of geological strength index (GSI).

5.2. Effect of Hoek-Brown Parameter m_i on Distribution of Fracture Zones. Figure 6 presents the distribution of fractures zones under various Hoek-Brown parameter m_i conditions when geological strength index (GSI) is 80. The other parameters are the same as mentioned in Section 4.

It can be seen from Figure 6 that when Hoek-Brown parameter m_i is greater than 10, only the width of fracture zones increases with the reduction of Hoek-Brown parameter m_i. While when Hoek-Brown parameter m_i is less than 10, both the number and the width of fracture zones increase with the reduction of Hoek-Brown parameter m_i.

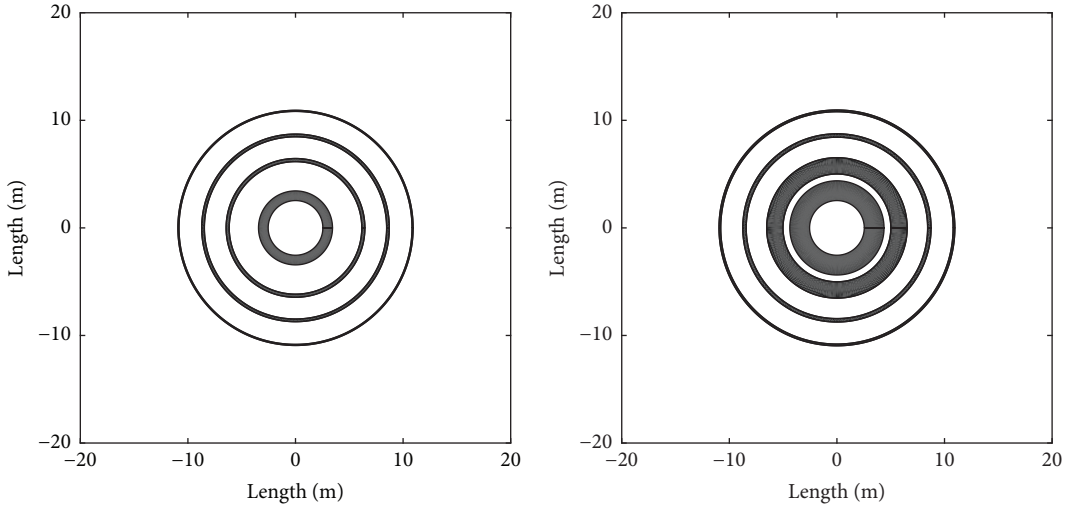

(a) High axial geostress (b) Coupled high axial geostress and blasting load

Figure 4: Zonal disintegration from present numerical computation result.

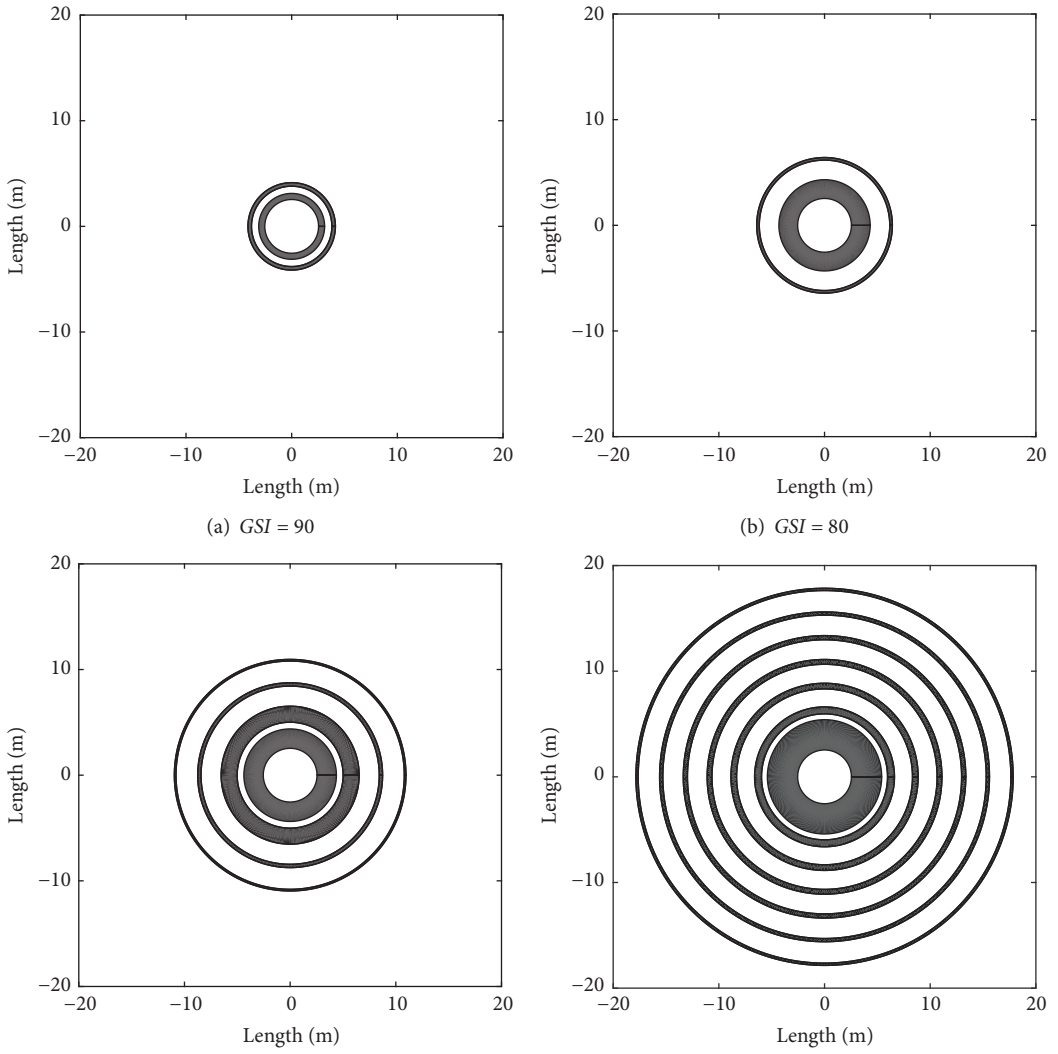

(a) $GSI = 90$ (b) $GSI = 80$

(c) $GSI = 75$ (d) $GSI = 70$

Figure 5: Effect of geological strength index (GSI) on zonal disintegration.

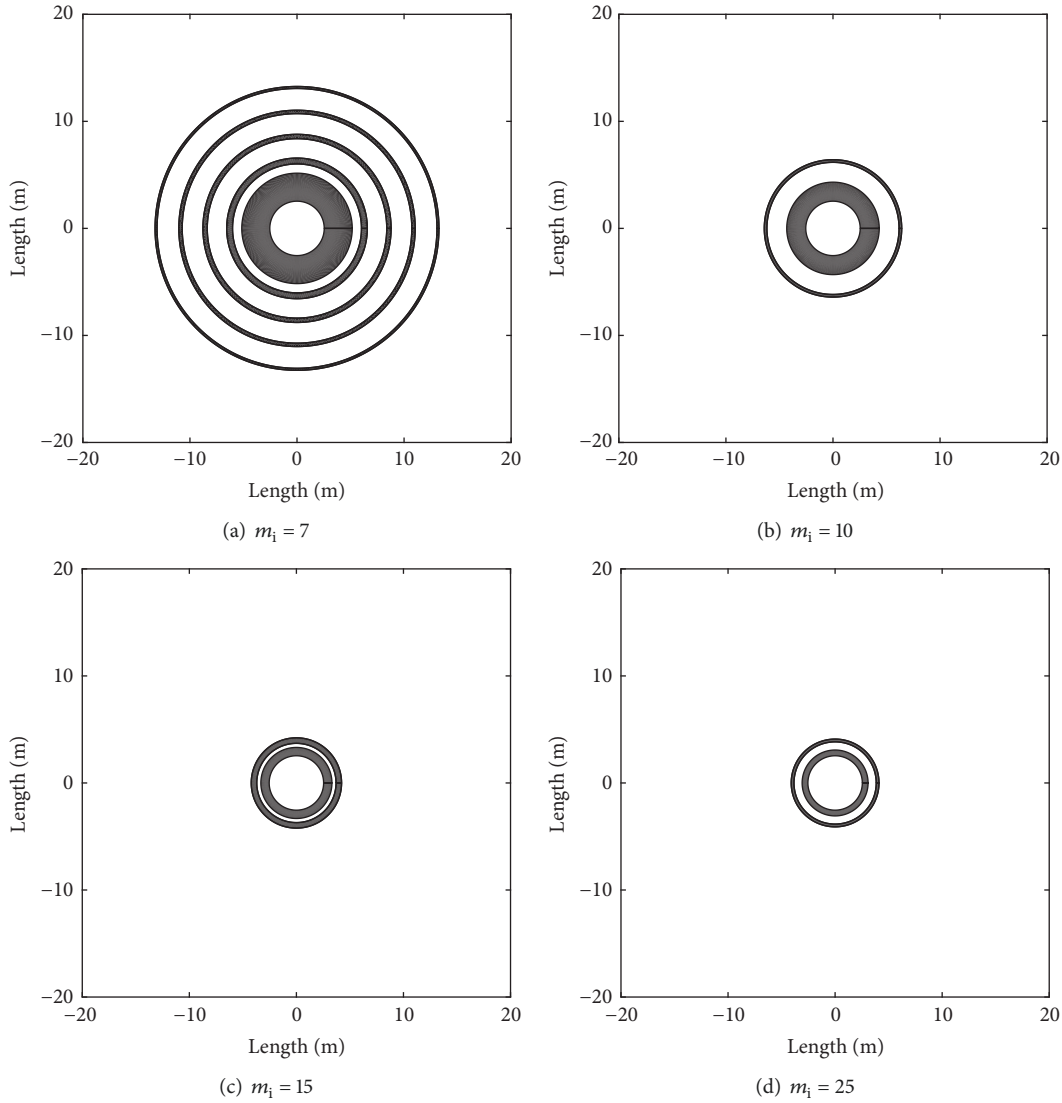

Figure 6: Effect of Hoek-Brown parameter m_i on zonal disintegration.

5.3. Effect of High Axial Geostress p_z on Distribution of Fracture Zones. As geological strength index (*GSI*) is 90 and Hoek-Brown parameter m_i is equal to 15, the distribution of fractures zones under various high axial geostress p_z conditions is shown in Figure 7. The other parameters are the same as mentioned in Section 4. High axial geostress p_z varies from 1 times to 1.6 times of uniaxial compressive strength of surrounding rock mass.

As seen from Figure 7, both the number and the width of fracture zones increase with the increase of high axial geostress p_z.

5.4. Effect of Peak Radial Blasting Load p_s on Distribution of Fracture Zones. When geological strength index (*GSI*) is equal to 80 and Hoek-Brown parameter m_i is equal to 10, the distribution of fractures zones under various peak radial blasting load conditions is shown in Figure 8. The other parameters are the same as mentioned in Section 4.

As seen from Figure 8, peak radial blasting load p_s, which decays in a negative exponential function, shows a small influence on the number of fracture zones but a relatively big effect on the width of fracture zone near the excavation.

6. Conclusions

As a characteristic failure in deep rock masses, zonal disintegration phenomenon is such a unique failure phenomenon with alternative distribution of fracture zones and nonfracture zones. To study the formation mechanism of zonal disintegration under coupled high axial geostress and blasting load, the elastic stress field distribution for a circular tunnel in deep isotropic rock masses is deduced by assuming that radial blasting load decays in a negative exponential function. And Hoek-Brown criterion is modified by assuming that blast-induced damage effect decays in a negative exponential function. With the deep tunnel of Dingji coal mine in China

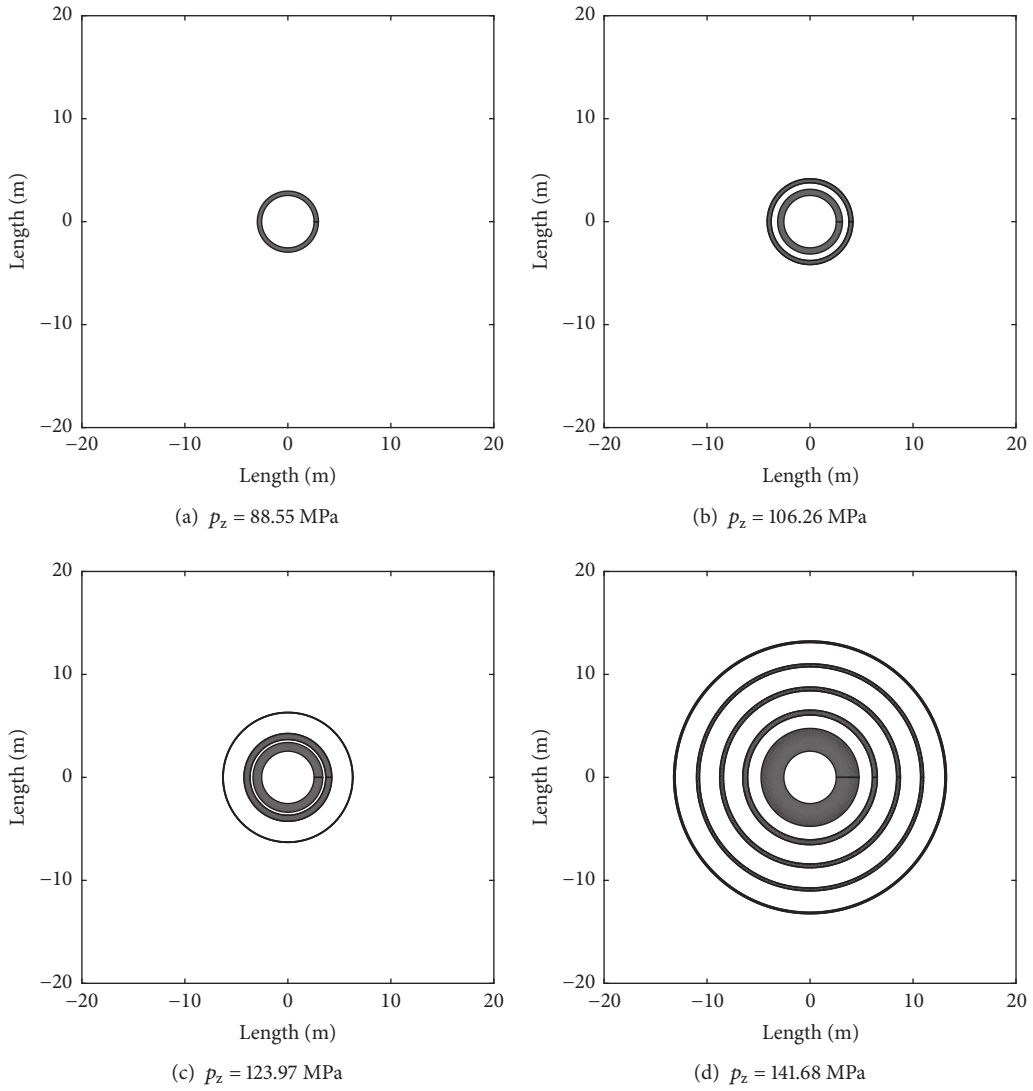

Figure 7: Effect of high axial geostress p_z on zonal disintegration.

as engineering background, the number and width of fracture zones are determined and they are in good accordance with the results observed in Dingji coal mine. Some numerical computations are carried out to study the effect of mechanical parameters of deep rock masses, high axial geo-stress, and radial blasting load on zonal disintegration. It is found that both the number and width of fracture zones mainly depend on high axial geostress and mechanical parameters of deep rock masses, and peak radial blasting load plays an important role in determining the width of fracture zone near the excavation. Both the number and the width of fracture zones increase with the increase of high axial geostress or with the deterioration of mechanical parameters of deep rock masses, while only the width of fracture zone near the excavation is extended with the increase of peak radial blasting load.

Data Availability

The datasets generated and analyzed during the current study are available from the corresponding author upon reasonable request.

Conflicts of Interest

The authors declare that there are no conflicts of interest regarding the publication of this paper.

Acknowledgments

This research is funded by the National Natural Science Foundation of China (no. 51174004 and no. 51774011), Anhui Natural Science Foundation (no. 1808085QE148), Natural Science Research Project of Colleges and Universities in

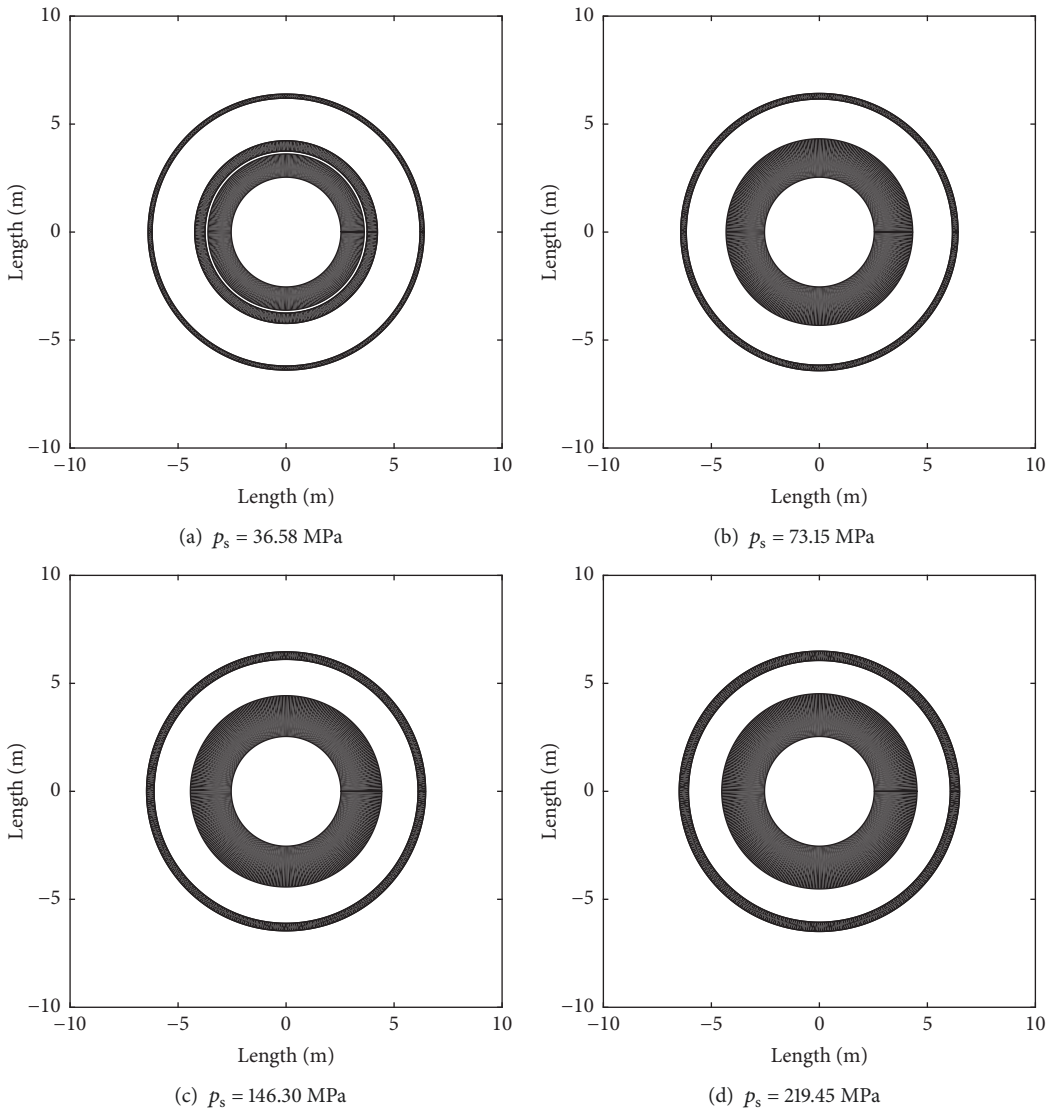

(a) p_s = 36.58 MPa (b) p_s = 73.15 MPa

(c) p_s = 146.30 MPa (d) p_s = 219.45 MPa

Figure 8: Effect of peak radial blasting load p_s on zonal disintegration.

Anhui Province (no. KJ2017A097), Young Teacher Scientific Research Project of Anhui University of Science and Technology (no. QN201607), and Science and Technology Project of Department of Housing and Urban-Rural Development of Anhui Province (no. 2017YF-08).

References

[1] C. Fairhurst, "Some Challenges of Deep Mining," *Engineering*, vol. 3, no. 4, pp. 527–537, 2017.

[2] H. P. Xie, F. Gao, Y. Ju et al., "Theoretical and technological conception of the fluidization mining for deep coal resources," *Journal of China Coal Society*, vol. 42, no. 3, pp. 547–556, 2017.

[3] X. Li, F. Gong, M. Tao et al., "Failure mechanism and coupled static-dynamic loading theory in deep hard rock mining: A review," *Journal of Rock Mechanics and Geotechnical Engineering*, vol. 9, no. 4, pp. 767–782, 2017.

[4] Q. H. Qian, X. P. Zhou, H. Q. Yang et al., "Zonal disintegration of surrounding rock mass around the diversion tunnels in Jinping II Hydropower Station, Southwestern China," *Theoretical and Applied Fracture Mechanics*, vol. 51, no. 2, pp. 129–138, 2009.

[5] X. Chen, T. Li, J. Xu et al., "Mechanism of zonal disintegration phenomenon (ZDP) and model test validation," *Theoretical and Applied Fracture Mechanics*, vol. 88, pp. 39–50, 2017.

[6] Q. Qian and S. Li, "A review of research on zonal disintegration phenomenon in deep rock mass engineering," *Chinese Journal of Rock Mechanics and Engineering*, vol. 27, no. 6, pp. 1278–1284, 2008.

[7] P. Yuan, *Model test on zonal disintegration in deep rock mass under blasting load*, Anhui University of Science and Technology, Huainan, 2016.

[8] G. R. Adams and A. J. Jager, "Petroscopic observations of rock fracturing ahead of stope faces in deep-level gold mines," *Journal of the South African Institute of Mining and Metallurgy*, vol. 80, no. 6, pp. 204–209, 1980.

[9] E. I. Shemyakin, G. L. Fisenko, M. V. Kurlenya et al., "Zonal disintegration of rocks around underground workings, Part I:

data of in situ observations," *Journal of Mining Science*, vol. 22, no. 3, pp. 157–168, 1986.

[10] S. C. Li, H. P. Wang, Q. H. Qian et al., "In-situ monitoring research on zonal disintegration of surrounding rock mass in deep mine roadways," *Chinese Journal of Rock Mechanics and Engineering*, vol. 27, no. 8, pp. 1545–1553, 2008.

[11] E. I. Shemyakin, G. L. Fisenko, M. V. Kurlenya et al., "Zonal disintegration of rocks around underground mines, part III: Theoretical concepts," *Journal of Mining Science*, vol. 23, no. 1, pp. 1–6, 1987.

[12] V. N. Odintsev, "Mechanism of the zonal disintegration of a rock mass in the vicinity of deep-level workings," *Journal of Mining Science*, vol. 30, no. 4, pp. 334–343, 1994.

[13] Q. Zhang, X. Zhang, Z. Wang et al., "Failure mechanism and numerical simulation of zonal disintegration around a deep tunnel under high stress," *International Journal of Rock Mechanics and Mining Sciences*, vol. 93, pp. 344–355, 2017.

[14] P. Jia, T. H. Yang, and Q. L. Yu, "Mechanism of parallel fractures around deep underground excavations," *Theoretical and Applied Fracture Mechanics*, vol. 61, pp. 57–65, 2012.

[15] L. Yuan, J. C. Gu, J. H. Xue et al., "Model test research on the zonal disintegration in deep rock," *Journal of China Coal Society*, vol. 39, no. 6, pp. 987–993, 2014.

[16] Z. Zhu, C. Wang, J. Kang et al., "Study on the mechanism of zonal disintegration around an excavation," *International Journal of Rock Mechanics and Mining Sciences*, vol. 67, pp. 88–95, 2014.

[17] X. P. Zhou, F. H. Wang, Q. H. Qian et al., "Zonal fracturing mechanism in deep crack-weakened rock masses," *Theoretical and Applied Fracture Mechanics*, vol. 50, no. 1, pp. 57–65, 2008.

[18] X. Zhou, Q. Qian, and B. Zhang, "Zonal disintegration mechanism of deep crack-weakened rock masses under dynamic unloading," *Acta Mechanica Solida Sinica*, vol. 22, no. 3, pp. 240–250, 2009.

[19] M. A. Guzev and A. A. Paroshin, "Non-Euclidean model of the zonal disintegration of rocks around an underground working," *Journal of Applied Mechanics and Technical Physics*, vol. 42, no. 1, pp. 131–139, 2001.

[20] X. Zhou and Q. Qian, "The non-Euclidean model of failure of the deep rock masses under the deformation incompatibilty condition," *Journal of Mining Science*, vol. 49, no. 3, pp. 368–375, 2013.

[21] Q. Qian and X. Zhou, "Quantitative analysis of rockburst for surrounding rocks and zonal disintegration mechanism in deep tunnels," *Journal of Rock Mechanics and Geotechnical Engineering*, vol. 3, no. 1, pp. 1–9, 2011.

[22] X. P. Zhou and J. Bi, "Zonal disintegration mechanism of cross-anisotropic rock mass around a deep circular tunnel under dynamic unloading," *Theoretical and Applied Fracture Mechanics*, vol. 60, no. 1, pp. 15–22, 2012.

[23] Q. Qian and X. Zhou, "Non-euclidean continuum model of the zonal disintegration of surrounding rocks around a deep circular tunnel in a non-hydrostatic pressure state," *Journal of Mining Science*, vol. 47, no. 1, pp. 37–46, 2011.

[24] X. P. Zhou, H. F. Song, and Q. H. Qian, "Zonal disintegration of deep crack-weakened rock masses: A non-Euclidean model," *Theoretical and Applied Fracture Mechanics*, vol. 55, no. 3, pp. 227–236, 2011.

[25] X. P. Zhou, G. Chen, and Q. H. Qian, "Zonal disintegration mechanism of cross-anisotropic rock masses around a deep circular tunnel," *Theoretical and Applied Fracture Mechanics*, vol. 57, no. 1, pp. 49–54, 2012.

[26] X. P. Zhou and Y. D. Shou, "Excavation-induced zonal disintegration of the surrounding rock around a deep circular tunnel considering unloading effect," *International Journal of Rock Mechanics and Mining Sciences*, vol. 64, pp. 246–257, 2013.

[27] Y. D. Shou, X. P. Zhou, and Q. H. Qian, "Dynamic model of the zonal disintegration of rock surrounding a deep spherical cavity," *International Journal of Geomechanics*, vol. 17, no. 6, pp. 1–11, 2017.

[28] H. Li, X. Xia, J. Li et al., "Rock damage control in bedrock blasting excavation for a nuclear power plant," *International Journal of Rock Mechanics and Mining Sciences*, vol. 48, no. 2, pp. 210–218, 2011.

[29] P. Yuan, Y. Xu, and J. Xue, "Model test of anchorage deep tunnel in blasting excavation," *Chinese Journal of Rock Mechanics and Engineering*, vol. 35, no. 9, pp. 1830–1836, 2016.

[30] J. Bi and X. P. Zhou, "Numerical simulation of zonal disintegration of the surrounding rock masses around a deep circular tunnel under dynamic unloading," *International Journal of Computational Methods*, vol. 12, no. 3, Article ID 1550020, 23 pages, 2015.

[31] Y. Xu and P. Yuan, "Model test of zonal disintegration in deep rock under blasting load," *Chinese Journal of Rock Mechanics and Engineering*, vol. 34, no. S2, pp. 3844–3851, 2015.

[32] Q. Ma, P. Yuan, J. Zhang et al., "Blast-induced damage on millisecond blasting model test with multicircle vertical blastholes," *Shock and Vibration*, vol. 2015, Article ID 504043, 6 pages, 2015.

[33] Y. J. Zuo, C. D. Ma, W. C. Zhu et al., "Model test study of mechanism of layered fracture within surrounding rock of tunnels in deep stratum tunnelling under dynamic disturbance," *Rock and Soil Mechanics*, vol. 32, no. 10, pp. 2929–2936, 2011.

[34] Q. Qian, X. Zhou, and E. Xia, "Effects of the axial in situ stresses on the zonal disintegration phenomenon in the surrounding rock masses around a deep circular tunnel," *Journal of Mining Science*, vol. 48, no. 2, pp. 276–285, 2012.

[35] W. Liu, W. Zhang, and S. H. Chen, "Study on cracking area of deep rock tunnel under blasting unloading," *Journal of Shandong University of Science and Technology (Natural Science)*, vol. 32, no. 2, pp. 66–70, 2013.

[36] E. Hoek and E. T. Brown, "Empirical strength criterion for rock masses," *Journal of Geotechnical and Geoenvironmental Engineering*, vol. 106, no. 9, pp. 1013–1035, 1980.

[37] H. Zhu, Q. Zhang, and L. Zhang, "Review of research progresses and application of Hoek-Brown strength criterion," *Chinese Journal of Rock Mechanics and Engineering*, vol. 32, no. 10, pp. 1945–1963, 2013.

[38] H. B. Chu, X. L. Yang, W. M. Liang et al., "Experimental study on the blast damage law of the simulated coal," *Journal of Mining and Safety Engineering*, vol. 28, no. 3, pp. 488–492, 2011.

[39] Q. Zhang, X. Zhang, W. Xiang et al., "Model test study of zonal disintegration in deep rock mass under different cavern shapes and loading conditions," *Chinese Journal of Rock Mechanics and Engineering*, vol. 32, no. 8, pp. 1564–1571, 2013.

[40] P. F. Zhang, Y. H. Su, K. X. Wang et al., "An approximate building method of ground reaction curve for non-circular underground caverns," *Hydrogeology and Engineering Geology*, vol. 42, no. 2, pp. 52–58, 2015.